Asia-Pacific Journal of Science and Technology: Volume: 27. Issue: 02. Article ID.: APST-27-02-09. Research Article

APST

Asia-Pacific Journal of Science and Technology

https://www.tci-thaijo.org/index.php/APST/index

Published by the Research and Graduate Studies,
Khon Kaen University, Thailand

Conversion of cassava rhizome to alternative biofuels via catalytic hydrothermal liquefaction

Parinvadee Chukaew[1,2], Kamonwat Nakason[1,2,*], Sanchai Kuboon[3], Wasawat Kraithong[3], Bunyarit Panyapinyopol[1,2] and Vorapot Kanokkantapong[4,5]

[1]Department of Sanitary Engineering, Faculty of Public Health, Mahidol University, Bangkok, Thailand
[2]Center of Excellence on Environmental Health and Toxicology (EHT), Bangkok, Thailand
[3]National Nanotechnology Center (NANOTEC), National Science and Technology Development Agency (NSTDA), Pathumthani, Thailand
[4]Department of Environmental Science, Faculty of Science, Chulalongkorn University, Bangkok, Thailand
[5]Research Group (STAR): Waste Utilization and Ecological Risk Assessment, the Ratchadaphiseksomphot Endowment Fund, Chulalongkorn University, Bangkok, Thailand
[*]Corresponding author: kamonwat.nak@mahidol.ac.th

Received 4 July 2021
Revised 24 September 2021
Accepted 5 October 2021

Abstract

In this study, cassava rhizome was converted to alternative biofuels including biocrude oil (BO) and hydrochar (HC) using catalytic hydrothermal liquefaction (C-HTL) at 250 and 300℃ for 15 min using 4.0 wt.% of K_2CO_3 as a catalyst. BO and HC properties were investigated regarding the parameters of elemental composition, chemical functional groups, chemical compositions, and surface morphology. The maximum energy recovery efficiency (ERE) of sum product (83.98 wt.%) was derived at 300℃. Therefore, 300℃ was suggested as a promising C-HTL temperature. This condition derived a yield of BO and HC at 33.70 and 33.29 wt.%, with their Higher heating value (HHV) at 26.45 and 18.81 MJ/kg, respectively. Gas chromatography - mass spectroscopy (GC-MS) analysis results indicated that BO principally contains phenols, aldehydes and ketones, hydrocarbons and alcohols which can be fractionated and upgraded into the biofuels and various valuable chemicals. The hydrogen/carbon (H/C) and oxygen/carbon (O/C) atomic ratios of BO and HC were similar to those of fossil fuel, indicating their high potential as fossil fuel substituting materials.

Keywords: Biocrude oil, Hydrochar, Biomass utilization, Renewable energy

1. Introduction

The rapid growth of the global economy has resulted in progressive fossil consumption, which has led to several huge drawbacks including unsustainability, environmental pollution, and disease [1]. Therefore, the search for alternative biofuels has received huge attention. Biomass is a sustainable and renewable material which can be used to produce the biofuels [2].

Cassava rhizome (CR) is one of the major biomasses of agricultural waste in Thailand and derived from cassava harvest. CR is commonly disposed of by an open burning process at plantations, resulting in several environmental problems such as air and soil pollutions. In 2020, Thailand produced 29 million tons of cassava product [3]. The CR residue product ratio is 0.2 [4]. Thus, the estimated amount of CR was 6 million tons. The major compositions of CR are hemicellulose, cellulose, and lignin which could be converted to various valuable products, especially fossil fuel replacing materials [5,6]. On the other hand, CR has high moisture content which could decrease its utilization efficiency [6].

Catalytic hydrothermal liquefaction (C-HTL) is the outstanding thermochemical conversion process for converting high moisture biomass to biofuels [7]. During C-HTL, water is used as a reaction medium, thus a pre-drying step for high moisture biomass is nonessential. The C-HTL operating conditions are normally mild

temperature (250-374℃) and high pressure (4-22 MPa) with or without catalysts [8]. The reaction sequence presented during biomass conversion using C-HTL includes hydrolysis, isomerization, defragmentation, depolymerization, and condensation reactions [9-11]. The biomass could be rapidly converted to biocrude oil (BO) and hydrochar (HC) [9]. BO is a major product from C-HTL which can be used as crude oil, and upgraded to gasoline and jet fuel [12,13]. HC is regarded as a by-product that can be used as an alternative coal [14]. K_2CO_3 presents outstanding activities for BO production using C-HTL [15-17]. It could substantially enhance the energy efficiency, inhibit solid residue formation, and reduce oxygen/carbon (O/C) atomic ratio [15,18]. Recently, several biomasses such as wheat husk [11], barley straw [15], and corn stalk [19] were converted to BO using the C-HTL process. However, the conversion of CR to BO through C-HTL process in the present of K_2CO_3 catalyst has yet to be conducted.

This study investigated the potential of alternative biofuel production from CR using the C-HTL process at 250 and 300℃ for 15 min using 4.0 wt.% of K_2CO_3 as a catalyst. The properties of BO and HC were investigated in the parameter of elemental compositions, chemical functional groups, chemical compositions, and surface morphology.

2. Materials and methods

2.1 Materials

CR was collected from Tha Muang District, Kanchanaburi Province, Thailand. CR was chopped and cleaned to remove any contaminants, then dried at 70℃ for 24 h. After that, the cleaned CR was pulverized to obtain CR powder with particles size smaller than 300 µm, and the powder was dried and stored over the methods in a related study [5,6,20]. The chemical compositions of CR powder are tabulated in Table 1 [21].

Table 1 Chemical compositions of CR powder [21].

Proximate analysis (wt.%, dry basis)		Ultimate analysis (wt.%, dry basis)	
Ash	8.32 ± 0.03	Carbon (C)	39.88 ± 0.17
Volatile matter	75.90 ± 0.40	Hydrogen (H)	5.39 ± 0.13
Fixed carbon	15.78 ± 0.42	Nitrogen (N)	0.80 ± 0.11
		Oxygen (O)	45.14 ± 0.37
		Higher heating value (HHV) (MJ/kg)	15.47 ± 0.22

2.2 Catalytic hydrothermal liquefaction experiments

The C-HTL experiments were conducted in a batch stainless-steel reactor (250 mL, VN supply Co., Ltd, Thailand) (Figure 1). In each batch experiment, 5 g CR powder, 4.0 wt.% of K_2CO_3 catalyst, and 50 mL distilled water were mixed in a glass vessel and placed in the reactor. After that, the reactor was tightly closed and heated in an electrical furnace at 250 and 300℃ for 15 min at 300 rpm stirring rate. After that, the reactor was immediately placed in a water bath for 30 min to quench the reaction. After that, BO was extracted using 250 mL ethyl acetate (EA) (conc. ≥ 99.9%). HC was isolated from the liquid by vacuum filtration using Whatman filter paper No.2. EA soluble product (BO) was separated from water soluble product (WSP) using a separatory funnel. And BO was separated from EA using a rotary evaporator. Each experiment was conducted in duplicate. In case any inconsistency was found (coefficient of variation was higher than 5%), a third one was performed. Predictive Analysis Software (PASW) statistics 18 was used to perform independent t-test at 95% confidence interval of different product yields and properties. The product samples were denoted as "TP-T" where TP represents type of products, and T represents the process temperature. For example, BO-250 stands for the BO sample obtained from C-HTL at 250℃.

2.3 Characterization and analysis

In this study, the elemental composition, chemical functional groups, chemical compositions, and surface morphology was analyzed. Elemental compositions (CHN) of the CR, BO, and HC were determined using an elemental analyzer (LECO CHN 628, USA). Oxygen (O) content was calculated by subtracting 100% from ash and elemental composition contents. Ash content was measured following the online standard analysis of NREL (NREL/TP-510-42622) [22]. Chemical functional groups of the CR, BO, and HC were observed through fourier-transform infrared spectroscopy (FTIR, Thermo Scientific Nicolet 6700, USA) using an infrared spectra wave number from 4000-600 cm^{-1} at 64 scans for a resolution of 4 cm^{-1} based on the attenuated total reflectance (ATR) method. Chemical composition of BO was identified using gas chromatography - mass spectrometry (GC-MS, GC 7890A/MS5975C, Agilent technologies, USA) equipped with HP-5MS column (30 m × 0.25 mm × 0.25 µm).

GC-MS was operated according to the following condition: hold at 40℃ for 4 min, ramp at 10℃/min to 280℃, and held at 280℃ for 20 min with the injector split ratio set to 30:1. Chemical species were determined through the NIST library. Surface morphology of CR and HC were observed using scanning electron microscopy (SEM, Quanta 250, Czech Republic).

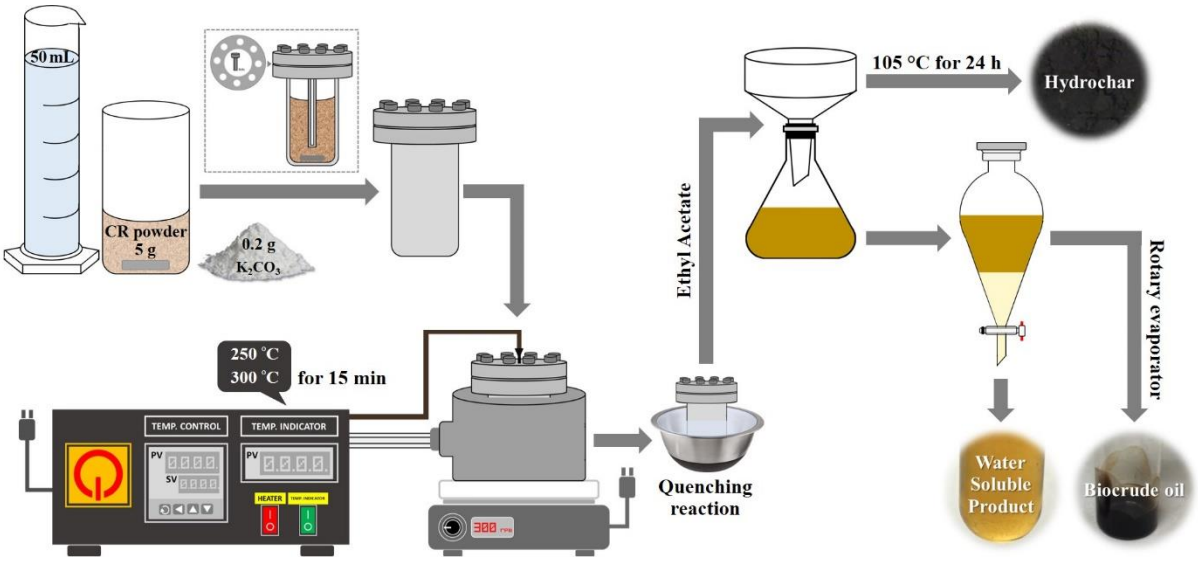

Figure 1 The schematic diagram of C-HTL experiments.

2.4 Calculation

BO, HC, and gas and other yields were calculated using Equation (1) - (3), respectively as shown below.

BO yield (wt.%, dry basis) = (mass of BO (g) / mass of dried raw CR (g)) × 100 (1)

HC yield (wt.%, dry basis) = (mass of HC (g) / mass of dried raw CR (g)) × 100 (2)

Gas and other yields (wt.%, dry basis) = 100 – (BO yield + HC yield) (3)

HHV of dried CR powder, BO, and HC was calculated using Dulong's formula [23] (Equation (4)).

HHV (MJ/kg) = 0.3491C + 1.1783H + 0.1005S – 0.1034O – 0.0151N – 0.021A (4)

where C, H, S, O, N, and A represent the percentages of carbon, hydrogen, sulphur, oxygen, nitrogen, and ash, respectively.

Energy recovery efficiency (ERE) was calculated using Equation (5).

ERE (wt.%) = (Product HHV / raw CR HHV) × BO yield (5)

3. Results and discussion

3.1 Product yields

Product yield is the vital parameter identifying the potential of biofuel production from C-HTL of CR. It identifies a portion of feedstock mass contained in the derived products through C-HTL process. Yields of BO, HC, and gas and other products derived from C-HTL of CR at 250 and 300℃ for 15 min using 4% K_2CO_3 as catalyst are illustrated in Figure 2. It presented that an increase in process temperature from 250 to 300℃ remarkably increased BO yield from 27.49 to 33.70 wt.% ($p < 0.05$), and decreased HC yield significantly from 33.29 to 21.30 wt.% ($p < 0.05$). In addition, increasing temperature also sharply increased gas and other product yield from 39.21 to 45.00 wt.% ($p < 0.05$). Similar trends were reported in C-HTL of corn stalk [19], and duckweed [24]. BO yield of corn stalk and duckweed increased from 14.35 to 23.32 wt.% and 5.4 to 9.7 wt.% with increasing process temperature from 270 to 290℃, respectively. As can be seen, BO yield of CR was higher than that of corn stalk and duckweed which could be due to the difference of lignocellulosic structures. An increase of process temperature enhances water ionic product (K_w) and biomass degradation severity, leading to BO formation, and hydrochar loss via hydrolysis, isomerization, defragmentation, depolymerization, and condensation reactions [11]. On the other hand, K_2CO_3 reacts with water and forms its bicarbonate (HCO_3^{2-}) and hydroxide (OH^-), which has been identified as an intermediate, and a secondary promoter in C-HTL, respectively [15,16]. These could weaken the intermolecular interaction of glucoside bonds in biomass [25]. Subsequently, depolymerization of biomass is promoted due to its low thermal stability with the addition of K_2CO_3, and thus producing more hydrolyzed

intermediate products in the aqueous phase. The greater the increase of these intermediates would result in a more aqueous phase, bio-crude and gaseous products through further reactions. These are the reasons for outstanding catalytic activities of K_2CO_3 in C-HTL.

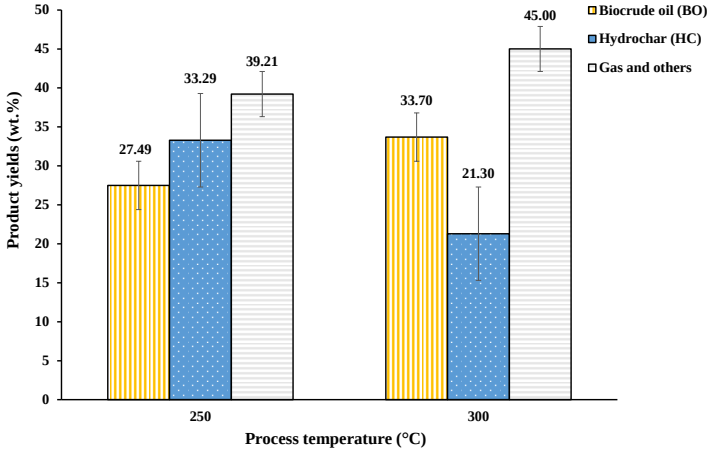

Figure 2 The schematic diagram of C-HTL experiment.

3.2 Product properties

Table 2 Elemental compositions and energetic properties of raw CR [21], BO, and HC.

Sample name	Element analysis (wt.%)				Ash (wt. %)	Atomic ratio		HHV (MJ/kg)	ERE (wt.%)
	C	H	N	O		H/C	O/C		
CR	39.88±0.17	5.39±0.11	0.80±0.13	45.14±0.37	8.32±0.03	1.61±0.03	0.85±0.01	15.47±0.22	NC
BO-250	54.95±0.00	6.72±0.00	1.61±0.00	36.72±0.00	ND	1.46±0.02	0.50±0.00	23.29±0.13	41.38±0.83
BO-300	59.91±1.28	7.46±0.13	1.42±0.01	31.22±1.16	ND	1.48±0.05	0.39±0.02	26.45±0.42	57.61±0.30
HC-250	48.09±0.31	4.50±0.11	1.10±0.02	28.03±0.53	18.09±0.08	1.11±0.02	0.44±0.01	18.81±0.29	40.48±0.45
HC-300	48.30±0.08	3.80±0.03	1.42±0.00	14.88±0.29	31.32±0.42	0.94±0.01	0.23±0.00	19.15±0.05	26.37±1.29

NC = Not calculated; ND = Not detected

Elemental compositions and energetic properties of raw CR, and products from C-HTL of CR are tabulated in Table 2. As can be seen, carbon content in BO and HC products were significantly higher than that of the CR ($p < 0.05$), and only marginally changed with process temperature ($p > 0.05$). On the other hand, oxygen contents of the products were significantly lower than that of raw CR ($p < 0.05$), and decreased repeatedly with process temperature ($p < 0.05$). The presence of these phenomena was primary due to dehydration and decarboxylation reactions [15]. On the other hand, ash content in HC increased significantly with increasing C-HTL temperature ($p < 0.05$), while ash content of BO was assumed to be ash free [15,26]. Increasing HC ash content was principally due to organic compositions dissolved and decomposed at a high rapid rate, thus the hydrochar product contained mainly ash proportion [27]. The changes of these elemental compositions resulted in raising HHV of BO and HC. Similar trends were reported in C-HTL of duckweed [24] and empty fruit bunches (EFB) [28]. HHV of BO from duckweed and EFB increased from 32.33 to 33.31 and 30.9 to 31.7 Mj/kg with increasing process temperature from 270 to 290℃ and 270 to 300℃, respectively. As can be seen, HHV of BO from duckweed and EFB was higher than that from CR which was due to the difference of lignocellulosic structures and content of each elemental composition.

ERE is calculated using product yield and its HHV. It presents the content of feedstock energy contained in the C-HTL product [6]. The maximum ERE of BO (57.61 wt.%) and HC (40.48 wt.%) could be obtained at 300 and 250℃, respectively. Furthermore, the maximum sum product ERE (83.98 wt.%) was derived at 300℃, thus this temperature was suggested as a promising temperature for producing biofuels through C-HTL of CR, corresponding to the promising C-HTL temperature of EFB [28], and birch sawdust [29]. The maximum EREs of BO from EFB, and birch sawdust were 36.14, and 63.8 wt.%, respectively. The H/C and O/C atomic ratio of CR, BO, and HC were depicted in the Van-Krevelen diagram (Figure 3). This diagram is an advantageous tool to indicate fuel properties of the biofuel materials. A material with the promising fuel properties is placed close to the beginning point [30]. It can be observed that H/C and O/C atomic ratios of BO and HC were substantially lower than those of CR ($p < 0.05$) which occurred due to deoxygenation reactions [15]. The atomic ratios of each product from different C-HTL temperatures were located in different areas. BO and HC with minimum H/C and O/C atomic ratios could be obtained through 300℃ C-HTL. In addition, H/C and O/C atomic ratios of that BO and HC were located close to fossil fuel indicating that BO and HC can be used as fossil fuel substituting material.

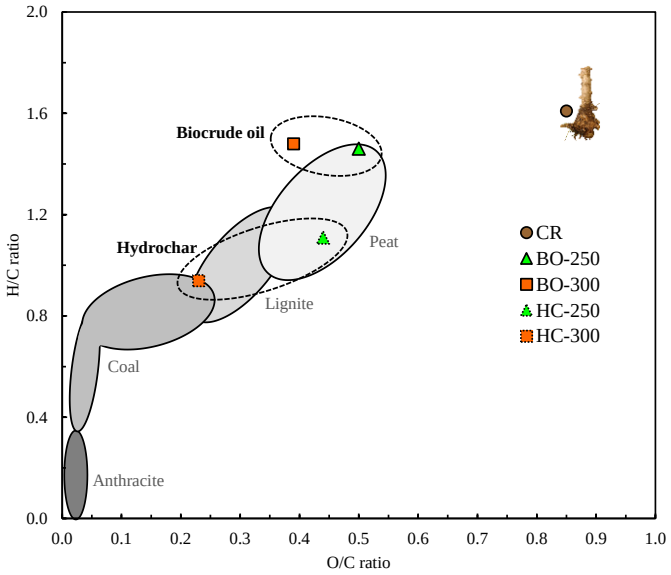

Figure 3 Van-Krevelen diagram of raw CR, BO, HC, and commercial coals [31].

3.3 Chemical functional groups

Chemical functional groups of CR, BO, and HC are illustrated over FTIR spectra in Figure 4. As can be seen, the spectra of raw CR substantially differed from BO, while slightly differing from HC. The broad transmittance bands, ranging from 3600 to 3200 cm^{-1}, were assigned to the -OH and C = O stretching vibration of hydroxyl and carbonyl groups ascribing to the presence of alcoholic, phenolic, and their derivative compounds. When comparing the intensity of this region, BO and HC had the lower intensity than that in raw CR, relating to reduced oxygen and hydrogen contents through the dehydration reaction [15]. The broad transmittance bands range from 3000 to 2800 cm^{-1} were ascribed to the C-H stretching vibration of aliphatic and aromatic structures. The intensity of this band in BO was higher than that in CR and HC implying that BO contained high aliphatic and aromatic structures compounds. The broad transmittance bands between 1710 and 1510 cm^{-1} were assigned to C = O stretching vibration of carboxyl and ester carbonyl groups. The intensity of these bands was strong in BO indicating that BO contained carboxylic acid and ester groups. The broad transmittance bands between 1370 and 1240 cm^{-1} were assigned to C-O stretching vibration in syringyl (1370 cm^{-1}) and guaiacol (1240 cm^{-1}) rings. The presence of these signals in BO indicated that it contained both syringyl and guaiacol compounds. The transmittance band at 1040 cm^{-1} was ascribed to the C-O, C = C and C-C-O stretching vibration of lignocellulose, which presented remarkably in CR and HC. The transmittance band at 757 cm^{-1} was assigned to C-H bending in the aromatic ring structure [32]. This band presented noticeably in BO indicating that BO had C-H aromatic ring structure.

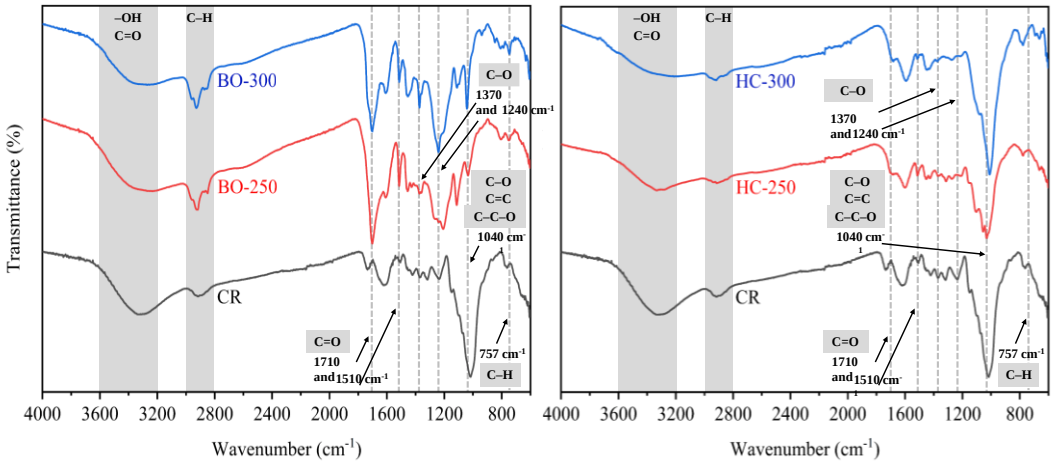

Figure 4 FTIR spectra of (A) BO and (B) HC.

3.4 Chemical compositions

Chemical compositions of BO are tabulated in Table 3, and could classified in seven groups regarding their functional groups (Figure 5), including aldehydes and ketones, phenols, alcohols, hydrocarbons, organic acids, amines, and esters. The major compositions of BO are phenols, aldehydes and ketones, hydrocarbons, and alcohol [33]. GC-MS analysis results indicated that BO had high phenols and hydrocarbons contents which could be fractionated and upgraded to petroleum-based chemicals and fossil fuels. The maximum content of phenols, and aldehydes and ketones could be achieved from C-HTL at 300°C. BO application and biofuel quality depend substantially on its chemical composition. Hydrocarbons can be classified as the non-polar fraction of the biofuel. BO with high hydrocarbon composition having carbon numbers predominantly in the range of C9 - C20 could be easily upgraded to diesel oil [34]. On the other hand, phenol can be classified as polar fraction of the biofuel. BO with high phenol composition could be easily upgraded to jet fuel [35].

Table 3 Chemical compositions of BO.

RT (min)	Compounds	Formular	Molecular Weight	% Area	
				250°C	300°C
Ketone/Aldehyde				31.27	33.13
5.38	Furfural	$C_5H_4O_2$	96.02	0.85	-
5.57	2-Cyclopenten-1-one	C_5H_6O	82.04	0.85	1.48
7.35	2-Cyclopenten-1-one,2-methyl-	C_6H_8O	96.06	3.42	8.44
7.37	Ethanone, 1-(2-furanyl)-(CAS)	$C_6H_6O_2$	110.04	1.96	-
7.41	2-ACETYL FURAN	$C_6H_6O_2$	110.04	-	0.91
8.00	2-Cyclopenten-1-one, 3, 4-dimethyl-	$C_7H_{10}O$	110.07	-	0.38
8.34	3-Ethylcyclopentanone	$C_7H_{12}O$	112.09	-	0.36
9.21	2,3-Dimethyl-2-cyclopenten-1-one	$C_7H_{10}O$	110.07	1.17	3.70
9.70	[(+)-(1r, 4s, 5s)-1-isopropyl-endo-4 methylbicyclo [3.1.0] hexan-3-0ne]	$C_{10}H_{16}O$	152.12	-	0.47
9.71	2-Cyclopenten-1-one, 2-hydroxy-3-methyl-	$C_6H_8O_2$	112.05	5.05	-
9.72	Spiro [2.4] heptan-4-one	$C_7H_{10}O$	110.07	-	0.57
9.95	5-Hydroxy-2-heptanone	$C_7H_{14}O_2$	130.10	-	2.74
10.01	2-Cyclopenten-1-one, 2, 3-dimethyl-	$C_7H_{10}O$	110.07	2.02	-
10.40	2-Cyclopenten-1-one, 3, 4, 4-trimethyl-	$C_8H_{12}O$	124.09	-	0.78
10.64	2-Cyclopenten-1-one, 3-ethyl-	$C_7H_{10}O$	110.07	1.64	1.31
10.87	Cyclohexanone, 2-isopropyl-2, 5-dimethyl-	$C_{11}H_{20}O$	168.15	1.15	-
11.03	5-Ethyl-2-furaldehyde	$C_7H_8O_2$	124.05	-	0.65
11.11	1H-Inden-1-one, 2, 3-dihydro-(CAS)	C_9H_8O	132.06	1.79	-
11.32	2-Cyclopenten-1-one, 3-ethyl-2-hydroxy-	$C_7H_{10}O_2$	126.07	3.36	-
11.72	3-Hexen-2-one, 3, 4-dimethyl-, (E) -	$C_8H_{14}O$	126.10	-	0.42
12.04	5, 8-Decadien-2-one, 5, 9-dimethyl-, (E) -	$C_{12}H_{20}O$	180.15	-	1.31
12.38	2-Acetonylcyclopentanone	$C_8H_{12}O_2$	140.08	-	0.82
12.47	2, 3-Dimethylhydroquinone	$C_8H_{10}O_2$	138.07	1.71	-
12.75	4, 5, 6, 6a-Tetrahydro-2(1H)-pentalenone	$C_8H_{10}O$	122.07	-	0.83
12.73	Bicyclo [3.2.1] octan-3-one, 6-hydroxy-, exo- (.+ -.)-	$C_8H_{12}O_2$	140.08	0.69	-
12.98	5-Hydroxymethylfurfural	$C_6H_6O_3$	126.03	0.26	-
13.33	2-Cyclohexen-1-one, 4, 4, 5-trimethyl-	$C_9H_{14}O$	138.10	1.26	-
13.56	(2-Methyl-cyclohex-2-enylidene) -acetaldehyde	$C_9H_{12}O$	136.09	-	0.74
13.76	2, 5-Diacetylfuran	$C_8H_8O_3$	152.05	-	3.81
13.81	4, 7-Methano-1H-indene-1, 8-dione, 3a, 4, 7, 7a -tetrahydro- (CAS)	$C_{10}H_8O_2$	160.05	-	1.29
14.25	2H-Inden-2-one, 1, 4, 5, 6, 7, 7a-hexahydro-7a-methyl-, (S) -	$C_{10}H_{10}O$	150.10	0.36	-
14.98	1-methoxy-4, 5, endo-8-trimethylbicylo [2.2.2] oct-5-en-2-one	$C_{12}H_{18}O_2$	194.13	0.96	-
14.98	4, 5, 6, 7, 8, 9-hexahydrocycloocta[c]furan-1(3H) -one	$C_{10}H_{14}O_2$	166.10	-	2.12
16.01	12-Oxatricyclo [4.4.3.0(1,6)] tridecane-3, 11-dione	$C_{12}H_{16}O_3$	208.11	0.56	-
17.08	2-Propanone, 1- (4-hydroxy-3-methoxyphenyl) -	$C_{10}H_{12}O_3$	180.08	2.22	-

Table 3 Chemical compositions of BO (cont.).

RT (min)	Compounds	Formular	Molecular Weight	% Area 250℃	% Area 300℃
Phenols				33.28	37.82
8.84	Phenol (CAS)	C_6H_6O	94.04	1.24	1.88
10.20	Phenol, 3-methyl-	C_7H_8O	108.06	2.80	2.49
10.81	Phenol, 2-methoxy- (CAS)	$C_7H_8O_2$	124.05	10.97	17.33
12.48	Creosol	$C_8H_{10}O_2$	138.07	-	3.60
14.76	Phenol, 2, 6-dimethoxy-	$C_8H_{10}O_3$	154.06	7.32	8.20
16.06	Phenol, 2-methoxy-4-(1-propenyl)-	$C_{10}H_{12}O_2$	164.08	2.16	0.71
16.80	2-tert-Butyl-4-isopropyl-5-methylphenol	$C_{14}H_{22}O$	206.17	7.87	3.60
19.03	Phenol, 2, 6-dimethoxy-4-(2-propenyl)-	$C_{11}H_{14}O_3$	194.09	0.92	-
Alcohols				12.47	9.99
9.15	Cyclohexanol, 2, 3-dimethyl-	$C_8H_{16}O$	128.12	-	1.29
10.40	(1, 3-DIMETHYL-2-METHYLENECYCLOPENTYL) METHANOL	$C_9H_{14}D_2O$	142.13	0.90	-
11.15	3-Pyridinol	C_5H_5NO	95.04	4.27	-
11.17	(R)-1-Cyclohexylethane-1, 2-diol	$C_8H_{16}O_2$	144.12	-	1.03
12.03	3-Pyridinol, 6-methyl-	C_6H_7NO	109.05	1.16	-
13.05	5-Caranol, trans,trans-(+)-	$C_{10}H_{18}O$	154.14	-	0.49
13.61	1, 4-Benzenediol (CAS)	$C_6H_6O_2$	110.04	-	0.66
13.76	4-isopropenyl-5-methyl-4-hexen-1-al	$C_9H_{14}O_2$	154.09	2.52	-
14.60	1, 4-Benzenediol, 2-methyl-	$C_7H_8O_2$	124.05	1.68	1.84
15.25	(7S) trans-anti-Tricyclo [7.3.0.0(2, 6)] dodecan-7-ol	$C_{12}H_{20}O$	180.15	0.75	-
15.25	1, 5:2, 4-Dimethanopentalene-3, 6-diol, octahydro-	$C_{10}H_{14}O_2$	166.10	-	1.01
15.61	(6-Hydroxymethyl-2, 3-dimethylphenyl) methanol	$C_{10}H_{14}O_2$	166.10	0.48	0.87
15.68	1, 3-Benzenediol, 4-ethyl-	$C_8H_{10}O_2$	138.07	-	1.71
17.00	2, 3, 5-Trimethoxytoluene	$C_{10}H_{14}O_3$	182.09	0.71	1.09
Hydrocarbons				20.62	12.78
7.57	7, 7-dimethyl-tetracyclo [4.1.0.0(2,4).0(3,3)] heptane	C_9H_{12}	120.09	0.87	-
9.16	Decane (CAS)	$C_{10}H_{22}$	142.17	1.26	-
9.82	1-Methylcyclooctene	C_9H_{16}	124.13	-	0.70
11.23	Cyclohexene, 1-methyl-4-(1-methylethyl)-, (R)-	$C_{10}H_{18}$	138.14	2.92	-
11.56	Bicyclo [2.2.2] octane, 2-methyl-	C_9H_{16}	124.13	-	0.36
12.55	Dodecane (CAS)	$C_{12}H_{26}$	170.20	2.91	2.57
15.35	Tetradecane	$C_{14}H_{30}$	198.23	4.66	3.65
15.69	1, 4-Dihydrothujopsene-(I1)	$C_{15}H_{26}$	206.20	0.35	-
17.73	1-Nonadecene (CAS)	$C_{19}H_{38}$	266.30	0.45	-
17.81	Hexadecane	$C_{16}H_{34}$	226.27	3.35	2.67
20.02	Octadecane (CAS)	$C_{18}H_{38}$	254.30	2.09	-
22.02	Docosane (CAS)	$C_{22}H_{46}$	310.36	1.24	2.82
23.86	Pentacosane (CAS)	$C_{25}H_{52}$	352.41	0.50	-
Organic acids				0.56	1.94
11.77	1H-Imidazole-4-carboxylic acid, 2-ethyl-	$C_6H_8N_2O_2$	140.06	-	1.16
12.97	Benzenesulfonic acid, 2-nitro-, methyl ester	$C_{10}H_{15}D_3O$	157.15	-	0.78
23.55	9, 12-Octadecadienoic acid (Z, Z)-	$C_{18}H_{32}O_2$	280.24	0.56	-
Amines				0.00	3.56
11.50	2-Methyl-4(5)-n-propylimidazole	$C_7H_{12}N_2$	124.10	-	0.25
14.44	(2, 6, 6-TRIMETHYLBICYCLO [3.1.1] HEPT-3-YL) METHANAMINE	$C_{11}H_{21}N$	167.17	-	0.89
16.01	Benzenamine, 2-methoxy-5-nitro- (CAS)	$C_7H_8N_2O_3$	168.05	-	1.12
17.08	(+)-s-2-Phenethanamine, 1-methyl-N-vanillyl-	$C_{17}H_{21}NO_2$	271.16	-	1.31
Esters				1.79	0.78
2.41	Propanoic acid, ethyl ester	$C_5H_{10}O_2$	102.07	1.21	0.78
21.32	METHYL-9, 9, 10, 10-D4-OCTADECANOATE	$C_{19}H_{34}D_4O_2$	302.31	0.58	-
Total				100.00	100.00

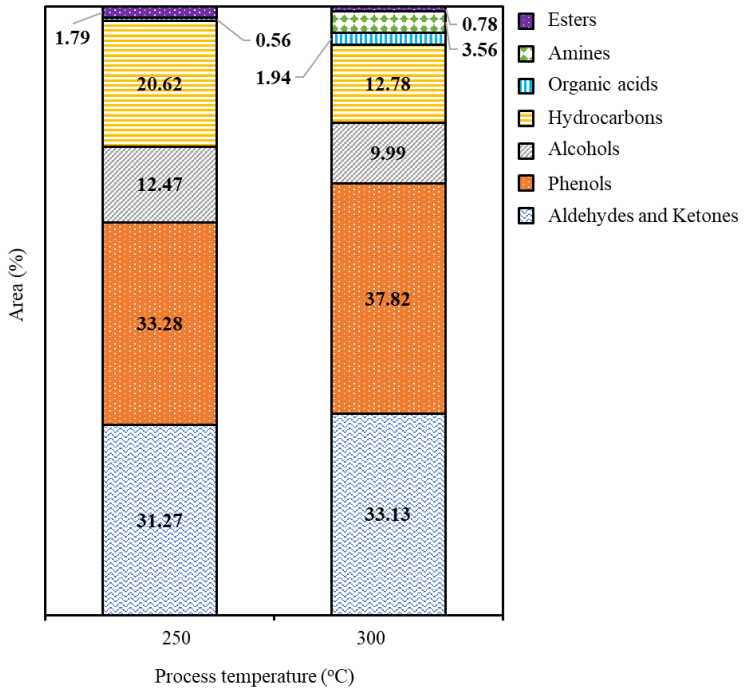

Figure 5 Chemical compositions of BO from C-HTL of CR.

3.5 Surface morphology

Surface morphology of raw CR and hydrochar derived from C-HTL at 250 and 300℃ is depicted in Figure 6. Figure 6(A) presents that the CR has a dense matrix and smooth surface. The morphology of HC from C-HTL at 250℃ was destroyed. It became broken, coarse, and porous (Figure 6B), At 300℃, the morphology was more cracked with pores (Figure 6C). These changes were mainly due to the devolatilization and depolymerization of the original CR, corresponding to reduced oxygen content in the elemental analysis results [6].

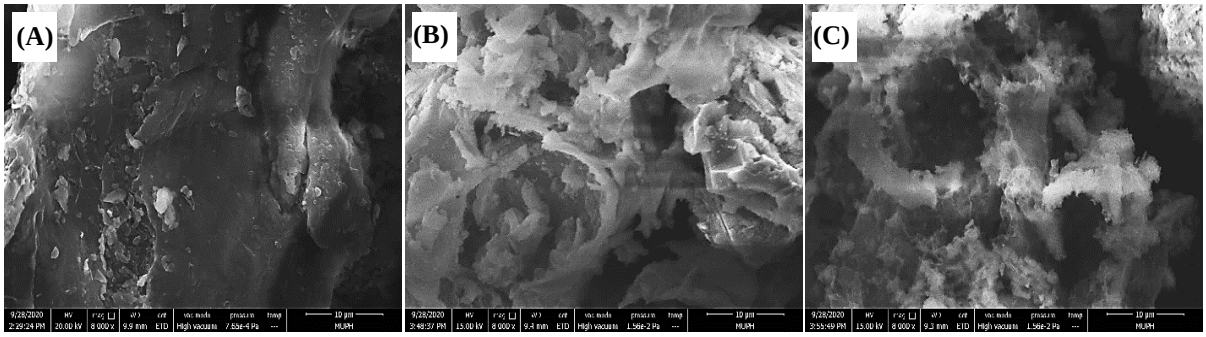

Figure 6 Surface morphology of (A) raw CR and HC from C-HTL of CR at (B) 250°C and (C) 300°C in 15 min.

4. Conclusion

C-HTL of CR was performed using 4.0 wt.% of K_2CO_3 at the process temperatures of 250 and 300℃ for 15 min. Process temperature substantially affected BO and HC properties. C-HTL at 300℃ derived the maximum ERE of sum product (83.98 wt.%). The energy related indexes and compositions of the final products indicated that both BO and HC can be used as alternative biofuels.

5. Acknowledgements

This work is supported by the 60th Year Supreme Reign of his Majesty King Bhumibol Adulyadej Scholarship, granted by the Faculty of Graduated Studies Aacademic Year 2018, Mahidol University and Funding from Program Management Unit on Competitiveness (Project no. P2052530). This work is supported for publication by the China Medical Board (CMB), Faculty of Public Health, Mahidol University, Bangkok, Thailand. Financial assistance for this research was also providing by the Center of Excellent on Environmental health and Toxicology (EHT), Bangkok, Thailand.

6. Conflicts of interest

The authors declare they have no competing financial interest.

7. References

[1] Tekin K, Karagöz S, Bektaş S. A review of hydrothermal biomass processing. Renew Sustain Energy Rev. 2014;40:673-687.

[2] Liu Y, Nie Y, Lu X, Zhang X, He H, Pan F, et al. Cascade utilization of lignocellulosic biomass to high-value products. Green Chem. 2019;21(13):3499-3535.

[3] Centre for Agricultural Information. Agricultural Production Data, http://www.oae.go.th/view/1/%E0%B8%82%E0%B9%89%E0%B8%AD%E0%B8%A1%E0%B8%B9%E0%B8%A5%E0%B8%81%E0%B8%B2%E0%B8%A3%E0%B8%9C%E0%B8%A5%E0%B8%B4%E0%B8%95%E0%B8%AA%E0%B8%B4%E0%B8%99%E0%B8%84%E0%B9%89%E0%B8%B2%E0%B9%80%E0%B8%81%E0%B8%A9%E0%B8%95%E0%B8%A3/TH-TH; 2019 [Accessed 30 June 2021]

[4] Ministry of Energy, Department of Alternative Energy Development and Efficiency. Biomass potential in Thailand, http://biomass.dede.go.th/biomass_web/index.html; 2013 [Accessed 30 June 2021].

[5] Nakason K, Panyapinyopol B, Kanokkantapong V, Viriya-empikul N, Kraithong W, Pavasant P. Characteristics of hydrochar and liquid fraction from hydrothermal carbonization of cassava rhizome. J Energy Inst. 2018;91(2):184-193.

[6] Nakason K, Khemthong P, Kraithong W, Chukaew P, Panyapinyopol B, Kitkaew D, et al. Upgrading properties of biochar fuel derived from cassava rhizome via torrefaction: effect of sweeping gas atmospheres and its economic feasibility. Case Stud Therm Eng. 2021;23:100823.

[7] Elliott DC. Hydrothermal liquefaction of sludge and biomass residues. In: Olivares JA, Puyol D, Melero JA, Dufour J, editors. Wastewater Treatment Residues as Resources for Biorefinery Products and Biofuels, Boston: Elsevier; 2020. p. 117-131.

[8] Gollakota ARK, Kishore N, Gu S. A review on hydrothermal liquefaction of biomass. Renewable Sustainable Energy Rev. 2018;81:1378-1392.

[9] Toor SS, Rosendahl L, Rudolf A. Hydrothermal liquefaction of biomass: a review of subcritical water technologies. Energy. 2011;36(5):2328-2342.

[10] Déniel M, Haarlemmer G, Roubaud A, Weiss-Hortala E, Fages J. Hydrothermal liquefaction of blackcurrant pomace and model molecules: understanding of reaction mechanisms. Sustainable Energy Fuels. 2017;1(3):555-582.

[11] Singh R, Bhaskar T, Dora S, Balagurumurthy B. Catalytic hydrothermal upgradation of wheat husk. Bioresour. Technol. 2013;149:446-451.

[12] Tzanetis KF, Posada JA, Ramirez A. Analysis of biomass hydrothermal liquefaction and biocrude-oil upgrading for renewable jet fuel production: the impact of reaction conditions on production costs and GHG emissions performance. Renewable Energy. 2017;113:1388-1398.

[13] Shamsul NS, Kamarudin SK, Rahman NA. Conversion of bio-oil to bio gasoline via pyrolysis and hydrothermal: a review. Renewable Sustainable Energy Rev. 2017;80:538-549.

[14] Zhang X, Gao B, Zhao S, Wu P, Han L, Liu X. Optimization of a “coal-like” pelletization technique based on the sustainable biomass fuel of hydrothermal carbonization of wheat straw. J Cleaner Prod. 2020;242:118426.

[15] Zhu Z, Toor SS, Rosendahl L, Yu D, Chen G. Influence of alkali catalyst on product yield and properties via hydrothermal liquefaction of barley straw. Energy. 2015;80:284-292.

[16] Akhtar J, Kuang SK, Amin NS. Liquefaction of empty palm fruit bunch (EPFB) in alkaline hot compressed water. Renewable Energy. 2010;35(6):1220-1227.

[17] Wang Y, Wang H, Lin H, Zheng Y, Zhao J, Pelletier A, et al. Effects of solvents and catalysts in liquefaction of pinewood sawdust for the production of bio-oils. Biomass Bioenergy. 2013;59:158-167.

[18] Karagöz S, Bhaskar T, Muto A, Sakata Y, Oshiki T, Kishimoto T. Low-temperature catalytic hydrothermal treatment of wood biomass: analysis of liquid products. Chem Eng J. 2005;108(1):127-137.
[19] Zhu Z, Si B, Lu J, Watson J, Zhang Y, Liu Z. Elemental migration and characterization of products during hydrothermal liquefaction of cornstalk. Bioresour Technol. 2017;243:9-16.
[20] Phachwisoot G, Nakason K, Chanthad C, Khemthong P, Kraithong W, Youngjan S, et al. Sequential production of levulinic acid and supercapacitor electrode materials from cassava rhizome through an integrated biorefinery process. ACS Sustainable Chem Eng. 2021;9(23):7824-7836.
[21] Chukaew P, Nakason K, Kuboon S, Kraithong W, Panyapinyopol B. Conversion of cassava rhizome to biocrude oil via hydrothermal liquefaction. Int Energy J. 2021;21(3):269-280.
[22] US national renewable energy laboratory. Determination of ash in biomass (NREL/TP-510-42622), https://www.nrel.gov/docs/gen/fy08/42622.pdf; 2005 [Accessed 30 June 2021].
[23] Channiwala SA, Parikh PP. A unified correlation for estimating HHV of solid, liquid and gaseous fuels. Fuel. 2002;81(8):1051-1063.
[24] Duan P, Chang Z, Xu Y, Bai X, Wang F, Zhang L. Hydrothermal processing of duckweed: effect of reaction conditions on product distribution and composition. Bioresour Technol. 2013;135:710-719.
[25] Rustamov VR, Abdullayev KM, Samedov EA. Biomass conversion to liquid fuel by two-stage thermochemical cycle. Energy Convers Manage. 1998;39(9):869-875.
[26] Yang L, Nazari L, Yuan Z, Corscadden K, Xu C, He Q. Hydrothermal liquefaction of spent coffee grounds in water medium for bio-oil production. Biomass Bioenergy. 2016;86:191-198.
[27] Nakason K, Panyapinyopol B, Kanokkantapong V, Viriya-empikul N, Kraithong W, Pavasant P. Hydrothermal carbonization of unwanted biomass materials: Effect of process temperature and retention time on hydrochar and liquid fraction. J Energy Inst. 2018;91(5):786-796.
[28] Lee JH, Hwang H, Choi JW. Effects of transition metals on hydrothermal liquefaction of empty fruit bunches (EFB) for conversion to biofuel and valuable chemicals. Energy. 2018;162:1-9.
[29] Malins K. Production of bio-oil via hydrothermal liquefaction of birch sawdust. Energy Convers Manage. 2017;144:243-251.
[30] Reza MT, Wirth B, Lüder U, Werner M. Behavior of selected hydrolyzed and dehydrated products during hydrothermal carbonization of biomass. Bioresour Technol. 2014;169:352-361.
[31] Basu P. Biomass Characteristics. In: Basu P, editor. Biomass Gasification, Pyrolysis and Torrefaction (Second Edition), Boston: Academic Press; 2013, p. 47-86.
[32] Zhang S, Zhou S, Yang X, Xi W, Zheng K, Chu C, et al. Effect of operating parameters on hydrothermal liquefaction of corn straw and its life cycle assessment. Environ Sci Pollut Res. 2020;27(6):6362-6374.
[33] Chen J. Bio-oil production from hydrothermal liquefaction of Pteris vittata L.: effects of operating temperatures and energy recovery. Bioresour Technol. 2018;265:320-327.
[34] Gad SC. Diesel Fuel. In: Philip W, editor. Encyclopedia of Toxicology (Second Edition), New York: Elsevier; 2005, p. 19-22.
[35] Zhu H, Janusson E, Luo J, Piers J, Islam F, McGarvey GB, et al. Phenol-selective mass spectrometric analysis of jet fuel. Analyst. 2017;142(17):3278-3284.